

Geophysical Research Letters®



RESEARCH LETTER

10.1029/2023GL103046

Key Points:

- We present detailed electron dynamics in guide-field reconnection at the center of a flux rope
- With $e\Phi_{\parallel} \geq kT_{e,\parallel}$, the observed electron behaviors can be well explained
- We suggest that electron beta is an important parameter for the generation of a large parallel electric field in guide-field reconnection

Correspondence to:







B.-B. Tang and W. Y. Li,
bbtang@spaceweather.ac.cn;
wyli@spaceweather.ac.cn

Citation:

Wang, H.-W., Tang, B.-B., Li, W. Y., Zhang, Y.-C., Graham, D. B., Khotyaintsev, Y. V., et al. (2023). Electron dynamics in the electron current sheet during strong guide-field reconnection. *Geophysical Research Letters*, 50, e2023GL103046. <https://doi.org/10.1029/2023GL103046>

Received 30 JAN 2023
Accepted 1 MAY 2023

Electron Dynamics in the Electron Current Sheet During Strong Guide-Field Reconnection

H.-W. Wang^{1,2}, B.-B. Tang¹ , W. Y. Li¹ , Y.-C. Zhang¹ , D. B. Graham³ , Y. V. Khotyaintsev³ , C.-H. Gao^{1,2} , X.-C. Guo¹, and C. Wang^{1,2}

¹State Key Laboratory of Space Weather, National Space Science Center, Chinese Academy of Sciences, Beijing, China,

²College of Earth and Planetary Sciences, University of Chinese Academy of Sciences, Beijing, China, ³Swedish Institute of Space Physics, Uppsala, Sweden

Abstract In this study, we investigate detailed electron dynamics in strong guide-field reconnection (the normalized guide field is ~ 1.5). This reconnection event is observed by the Magnetospheric Multiscale (MMS) spacecraft at the center of a flux rope in the magnetotail. With the presence of a large parallel electric field (E_{\parallel}) in the electron current sheet, electrons are accelerated when streaming into this E_{\parallel} region from one direction, and decelerated from the other direction. Some decelerated electrons can reduce the parallel speed to ~ 0 to form relatively isotropic electron distributions at one side of the electron current sheet, as the estimated acceleration potential satisfies the relation $e\Phi_{\parallel} \geq kT_{e,\parallel}$, where $T_{e,\parallel}$ is the electron temperature parallel to the magnetic field. Therefore, a large E_{\parallel} is generated to balance the parallel electron pressure gradient across the electron current sheet, since electrons at the other side of the current sheet are still anisotropic. Based on these observations, we further show that the electron beta is an important parameter in guide-field reconnection, providing a new perspective to solve the large parallel electric field puzzle in guide-field reconnection.

Plain Language Summary Magnetic reconnection is a universal process that rapidly converts energy from the magnetic field to plasma. The energy conversion at kinetic scales is of particular interest to researchers, as it is directly related to reconnection process in the central diffusion region. In general, the reconnecting magnetic fields do not have to be antiparallel, and an additional magnetic component known as the guide field (B_g) can appear in the direction perpendicular to the reconnecting plane. Recently, observations from Magnetospheric Multiscale (MMS) mission show a large electric field parallel to the local magnetic field, which is several times larger than the reconnection electric field, can appear in guide-field reconnection, and impact electrons significantly. However, the generation of this large parallel electric field in strong guide-field reconnection is still not fully understood. In this study, we suggest that the electron beta (ratio of the electron thermal pressure to the magnetic pressure) is an important parameter in guide-field reconnection. Only within some proper electron beta range, a parallel pressure gradient across the electron current sheet can form to balance the large parallel electric field.

1. Introduction

Magnetic reconnection is a fundamental process with explosive energy conversion from magnetic fields to plasmas and rapid reconfiguration of magnetic field lines. In general, the reconnecting magnetic fields do not have to be antiparallel, and an additional magnetic component known as the guide field (B_g) can appear in the direction perpendicular to the reconnecting plane. With the increase of B_g , the guide field can gradually magnetize electrons in the central diffusion region (e.g., Le et al., 2013), resulting into the transition from antiparallel to guide-field reconnection (Swisdak et al., 2005). In guide-field reconnection, B_g can cause the diamagnetic drift of the X-line, which may eventually suppress reconnection (e.g., Phan et al., 2013; Swisdak et al., 2003). The reconnection current sheet is deflected by the $J_L \times B_g$ force (J_L is the current along the reconnecting direction, Goldman et al., 2011; Tang et al., 2022), and the Hall field structure is accordingly distorted (Eastwood et al., 2010). The reconnection electric field becomes parallel to the guide field in the vicinity of the X-line, which leads to the shift of the local energy conversion location to the magnetic field reversal points (Genestreti et al., 2017) and the significance of parallel energy dissipation (Wilder et al., 2018). In addition, this parallel electric field (E_{\parallel}) can accelerate electrons from one direction, and decelerate electrons from the other direction, forming a density cavity on one edge of the exhaust (Eastwood et al., 2018) and electron beams that are unstable for electron beam-type instabilities (e.g., Drake et al., 2003; Khotyaintsev et al., 2020; Tang et al., 2020).

© 2023 The Authors.

This is an open access article under the terms of the [Creative Commons Attribution-NonCommercial License](https://creativecommons.org/licenses/by-nc/4.0/), which permits use, distribution and reproduction in any medium, provided the original work is properly cited and is not used for commercial purposes.

Recently, with the high resolution data from Magnetospheric Multiscale (MMS) mission (Burch et al., 2016), it is found that E_{\parallel} tends to increase with B_z , which can be several times larger than the reconnection electric field (E_R) (Wang et al., 2021; Wilder et al., 2017, 2018). This large E_{\parallel} is balanced by the electron pressure gradient in an MMS event study (Wilder et al., 2017). As revealed from a kinetic simulation of moderate guide field reconnection, E_{\parallel} is suggested to be balanced by the parallel electron pressure gradient caused by a transition between isotropic and anisotropic electrons at the two sides of the electron jet (Wetherton et al., 2022). However, the generation of this E_{\parallel} in strong guide-field reconnection is still not fully understood. Meanwhile, E_{\parallel} is related to an acceleration potential (Φ_{\parallel}), whose magnitude is key to impact electrons. Wilder et al. (2017) suggests that the electrons can be accelerated by Φ_{\parallel} when passing through it from one direction, and the accelerated electrons can be immediately reflected after exiting the acceleration region due to the developed electron streaming instability, but the detailed electron reactions to this acceleration potential is still lacking due to the limited spatio-temporal resolution of data.

Reconnection at the center of a magnetic flux rope is typical for guide-field reconnection, which occurs when a thin current sheet is formed due to the magnetic flux compression from two sides (Kacem et al., 2018; Øieroset et al., 2016, 2019). In this study, we focus on such a reconnection event in the magnetotail as previously reported by X. Li et al. (2022), and show detailed electron reactions to a large acceleration potential ($\Phi_{\parallel} \sim 2$ kV), as the scale length (i.e., the electron inertial length) in the magnetotail is relatively large. We also propose a quantitative relation for Φ_{\parallel} , and finally indicate that the electron β (ratio of the electron thermal pressure to the magnetic pressure) can be an important parameter to generate a large E_{\parallel} in the guide-field reconnection.

2. Observation

We present MMS observations at Earth's magnetotail on 02 August 2020, and we use magnetic field data from the fluxgate magnetometer (Russell et al., 2016), electric field data from the electric field double probes (Ergun et al., 2016; Lindqvist et al., 2016), and particle data from the fast plasma investigation (Pollock et al., 2016). Figure 1 provides an overview of the Earth's magnetotail between 16:35:00 UT and 17:30:00 UT from MMS 1. At this time, the four MMS spacecraft are located at $[-28.09, -2.70, 3.51]$ Earth radii (R_E) in geocentric solar magnetospheric (GSM) coordinates, and the spacecraft are in a tetrahedron formation with ~ 36 km separation. MMS 1 is initially located at the north side of the plasma sheet characterized by a large positive B_x , then crosses the plasma sheet for several times with the sign change of B_x , and finally return to the northern side of the plasma sheet (Figure 1a). The ion density (Figure 1b) and energy spectrum (Figure 1d) also present typical signatures of the plasma sheet, and clear magnetic field fluctuations (Figure 1a) suggest this plasma sheet is highly turbulent. The X-component of \mathbf{V}_{ion} reversals from negative (tailward) to positive (Earthward) during this time interval (Figure 1c), which is taken as an indicator for ongoing magnetic reconnection that is retreating tailward. A schematic of the MMS trajectory relative to magnetic reconnection is shown in Figure 2a.

During the tailward ion flow (shaded in yellow in Figures 1a–1c), MMS observes a magnetic bipolar structure around 16:56:15 UT (Figure 2b). By reconstructing this structure from the Grad-Shafranov method (Sonnerup et al., 2006; Zhang et al., 2007), a magnetic flux rope is revealed (Figure 1e). The size of this flux rope along the MMS trajectory is about 5,000 km or 6.9 ion inertial lengths (d_i) based on the local ion number density at $\sim 0.1 \text{ cm}^{-3}$ (Figure 1f). The two edges of this flux rope can also be inferred from variations of electron pitch angle spectrum (Figure 1i), showing consistent results with reconstructions. The reconstructed magnetic flux rope is not cylindrical, which is significantly compressed along MMS trajectory. This can be attributed to the difference of the flow speed at the two sides of the B_z reversal (Figure 1g). More detailed descriptions of this event have been presented in X. Li et al. (2022). We note that due to this compression effect, a thin current sheet, featured by large electron flows (Figure 1h), is formed at the center of the flux rope, which is the focus of this study.

A zoom-in of this current sheet is presented in boundary-normal (LMN) coordinates (Figure 3), which is determined by a hybrid variance analysis method. First, the out-of-plane direction (\mathbf{M}) satisfies that $\mathbf{M} \parallel (\mathbf{B}_1 + \mathbf{B}_2) \times (\mathbf{B}_1 - \mathbf{B}_2) \times (\mathbf{B}_1 - \mathbf{B}_2)$, where \mathbf{B}_1 and \mathbf{B}_2 are the averaged magnetic field at the two sides of the current sheet. Here, we use $\mathbf{B}_1 = [3.06, 15.08, 2.46]$ nT from the time interval from 16:56:14.20 to 16:56:14.40 UT, and $\mathbf{B}_2 = [-2.71, 9.54, -11.25]$ nT is taken from 16:56:14.90 to 16:56:15.10 UT. The normal direction (\mathbf{N}') is along the minimum variance direction of the current density (16:56:14.40 to 16:56:14.90 UT), and $\mathbf{L} = \mathbf{M} \times \mathbf{N}'$. Finally, \mathbf{N} completes the right-handed system. In GSM, it gives $\mathbf{L} = [0.08 \ 0.37 \ 0.92]$, and $\mathbf{M} = [-0.00 \ 0.93 \ -0.37]$ and $\mathbf{N} = [-0.99 \ 0.03 \ 0.07]$, respectively. The advantage of this hybrid method is that we can get almost equal B_M at the two sides of the current sheet. The electron velocity and the electric field are presented in the ion-rest frame,

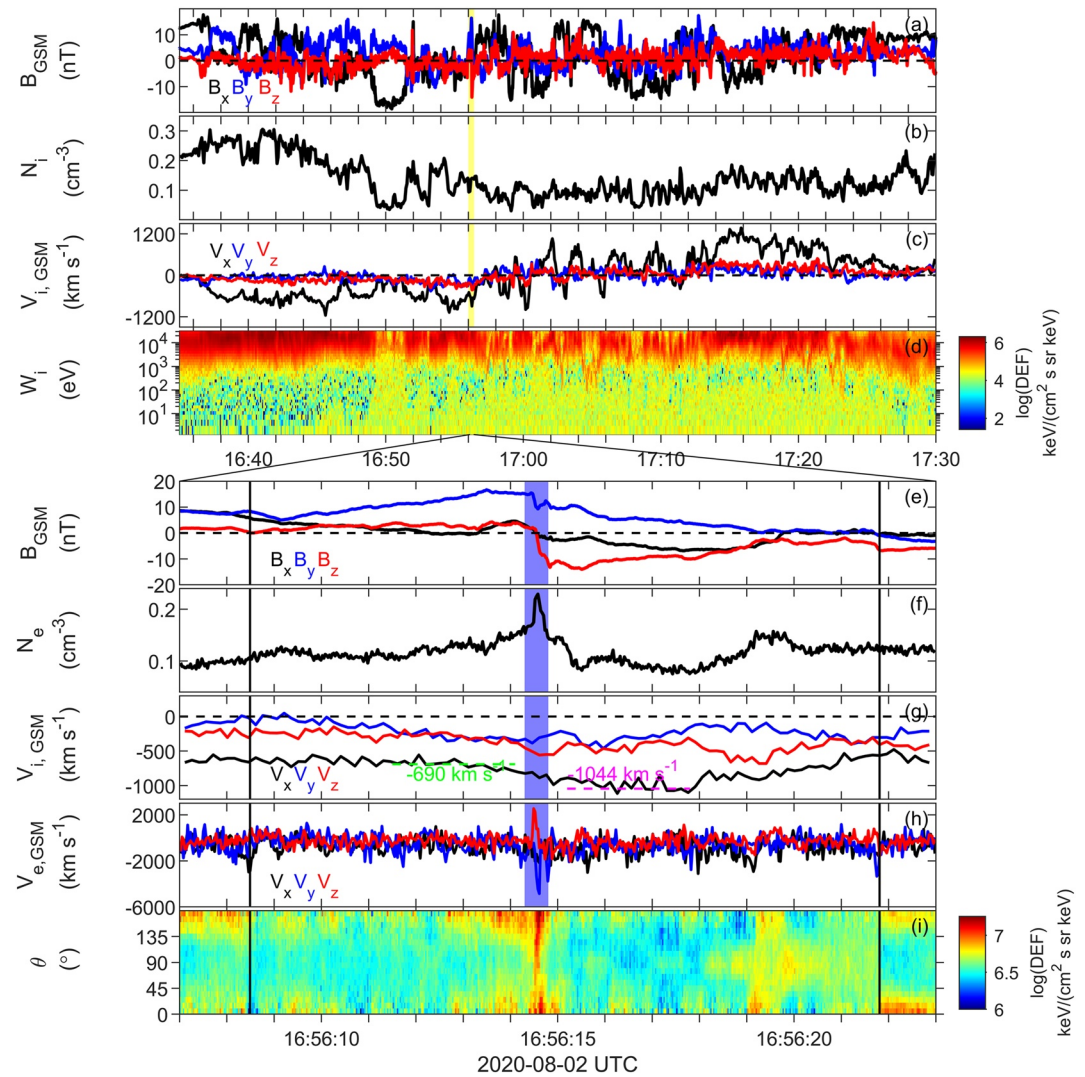


Figure 1. Overview of the Earth's magnetotail on 02 August 2020 from MMS 1. Panels show (a) magnetic field, (b) ion number density, (c) ion bulk velocity, (d) ion omnidirectional differential energy flux. Zoom-in of (e) magnetic field, (f) electron number density, (g) ion bulk velocity, (h) electron bulk velocity and (i) electron pitch angle spectrum. All vectors are shown in geocentric solar magnetospheric coordinates.

as the ion flow speed is large and steady during this time interval (not shown). Actually, the speed of this current sheet along the normal direction (V_N) is $\sim 900 \text{ km s}^{-1}$ from the four-spacecraft timing analysis of B_L . During this current sheet crossing, MMS observe clear bipolar Hall electric fields (Figure 3b) and fast electron bulk flows in the +L direction (Figure 3e), which are consistent with reconnection (X. Li et al., 2022). The background B_M ($\sim 13 \text{ nT}$) is about 1.5 times larger than the reconnecting B_L ($\sim 8\text{--}9 \text{ nT}$, Figure 3a), indicating a strong guide field ($B_g/B_L \sim 1.5$). The measured maximum parallel electric field (E_{\parallel}) during the current sheet crossing is about 7.5 mV m^{-1} , and its mean value (averaged between the shaded magenta and cyan region) is about 4 mV m^{-1} . Although the observed E_{\parallel} is much larger than the estimated reconnection electric field ($E_R \sim 0.1 V_{A, \text{in}} B_{L, \infty} \sim 0.4 \text{ mV m}^{-1}$), we note the E_{\parallel} measurements have large uncertainties (shaded in green in Figure 3c), and additional evidence are provided later from electron observations. The width of this current sheet, estimated from the peak values of E_N , is about 270 km . In this event, the ion inertial length is about 520 km , while the electron inertial length is about 13 km , suggesting the current sheet is between ion and electron scales, allowing us to investigate detailed electron dynamics in guide-field reconnection.

Due to the presence of E_{\parallel} , electrons undergo acceleration/deceleration once entering the E_{\parallel} region (Figure 2c). Electron pitch angle—energy distributions around the B_L reversal are presented (Figures 2i–2n). From the left

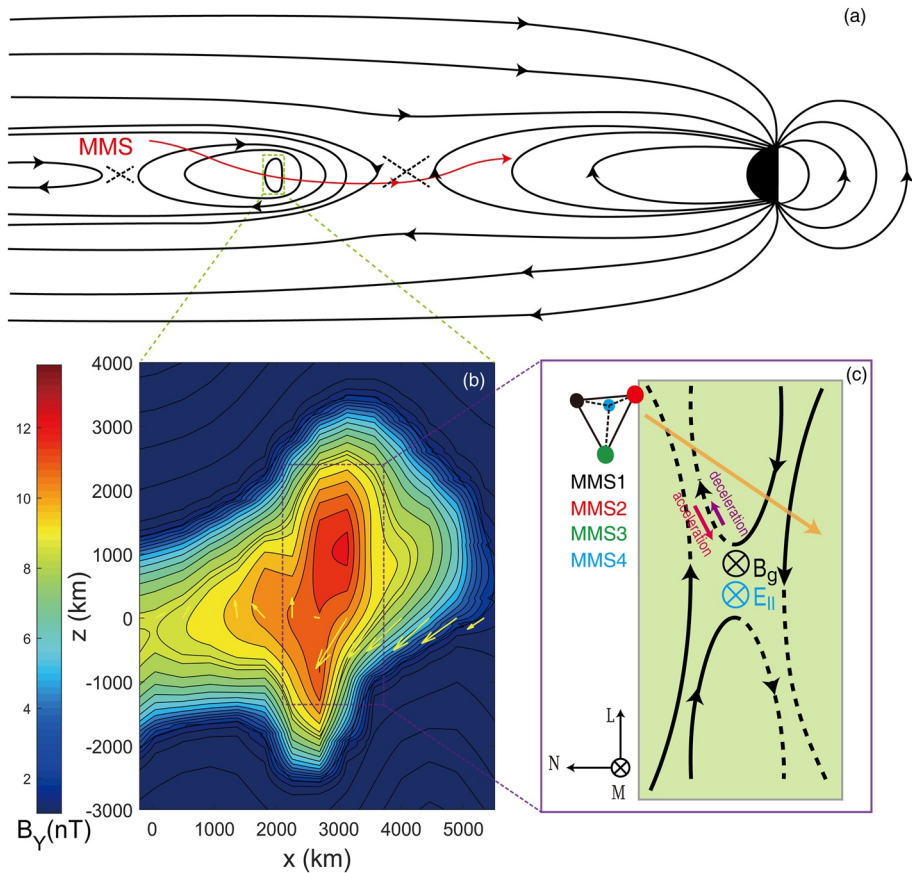


Figure 2. Schematic of MMS observations in the Earth's magnetotail on 02 August 2020. Panels show (a) a cartoon of the magnetotail reconnection and the MMS trajectory relative to reconnection, (b) the magnetic flux rope reconstructed from the Grad-Shafranov method, and (c) two-dimensional schematic of the guide-field reconnection at the flux rope center. In panel (b), the colored contours present the reconstructed out-of-plane B_y component, and the yellow arrows show the in-plane magnetic field vectors along the MMS path. In panel (c), the orange line shows the MMS trajectory in reconnection, and the black lines are magnetic field lines. The red/purple arrows presents the accelerated/decelerated electrons entering the $E_{||}$ region from two sides.

to right, electrons that are anti-parallel to the magnetic field are gradually accelerated to form electron beams around 180° pitch angles (shaded in cyan). Meanwhile, the parallel electron beam that enters the $E_{||}$ region from the right would be decelerated, leading into the increase of electron pitch angles, and the formation of nearly isotropic electron distributions at the left side (shaded in magenta). The disappearance of the parallel electron beam suggests the potential drop ($\Phi_{||}$) inside the $E_{||}$ region is sufficiently large in magnitude, that is, it is larger than the electron thermal energy ($e\Phi_{||} \geq kT_{e,||}$), so that electrons can effectively reduce the parallel speed and even turn around to generate isotropic electron distributions. Once electrons become more isotropic, a density peak would appear (Figure 3d) and the isotropic electrons are convected away with the magnetic field lines to form electron outflows (Figure 3e).

To further confirm the electron dynamics observed in the guide-field reconnection, quantitative evidence are presented in Figure 4. It is noted that MMS 3 shows a last-in-first-out feature during the current sheet crossing and the magnetic B_M dip is shallowest at MMS 3 (Figures 4a and 4c), indicating that MMS 3 is the closest spacecraft to the reconnection X-line. However, only high-resolution electron data from MMS 1 and 2 are available during this time interval, which are presented in this figure. Figure 4d shows electrons are roughly magnetized in this event as the magnetic curvature radius is much larger than the electron thermal gyro-radius and Figure 4e shows the electron firehose condition is not satisfied as the ratio of $\mu_0(P_{||} - P_{\perp})/B^2$ is small. Therefore, we conclude that the parallel electric field is the primary factor for electron dynamics. We also calculate the electron partial density at different pitch angles, that is, $0-45^\circ$ (Figure 4i), $45^\circ-135^\circ$ (Figure 4h) and $135^\circ-180^\circ$

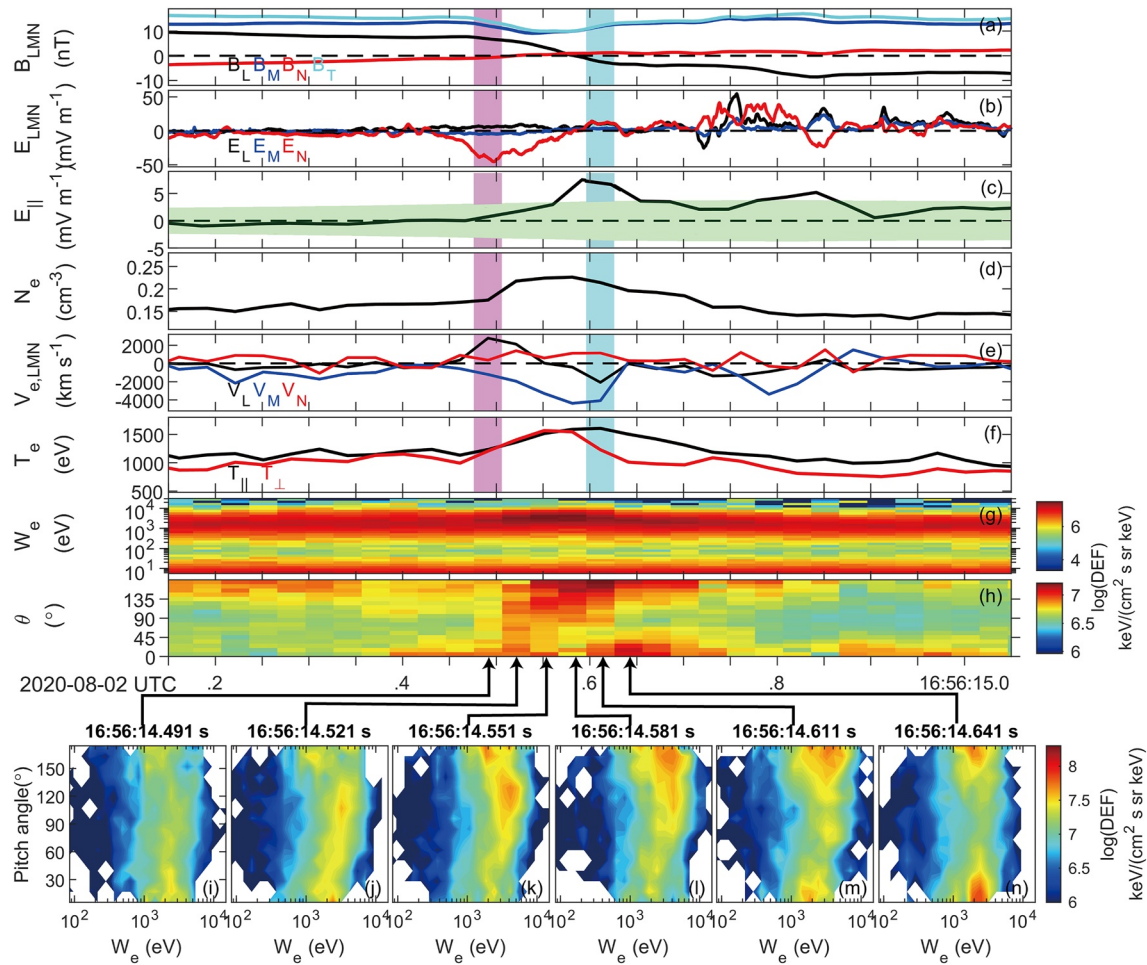


Figure 3. MMS 1 observations of guide-field reconnection at the center of a flux rope. From the top, panels are (a) \mathbf{B} , (b) the burst mode \mathbf{E} , (c) $E_{||}$ in the fast mode, (d) n_e , (e) \mathbf{V}_e , (f) $T_{e,\perp}$ and $T_{e,||}$, (g) electron omnidirectional differential energy flux and (h) electron pitch angle spectrum. \mathbf{E} and \mathbf{V}_e have been transferred into the ion-rest frame, and all vectors are shown in LMN coordinates. (i–n) electron pitch angle-energy distributions at six consecutive sampling time as indicated by black arrows.

(Figure 4j). Their sums are presented with dashed lines in Figure 4g, which are nearly identical with published data (solid lines in Figure 4g). It is shown that the electron density near 90° pitch angles increases between the shaded magenta and cyan region, responsible for the variation of the total density. This result suggests that $\Phi_{||}$ can sufficiently decelerate the parallel-moving electrons, and even reduce the parallel speed of some electrons to ~ 0 . We directly infer $\Phi_{||}$ by comparing the electron phase space density at 180° pitch angles at the time shaded in magenta and cyan (Figure 4k) from Liouville's theorem. The dotted green line, which is energy shifted from the red, is the best fit of the black line. The shifted energy is taken as $\Phi_{||}$, which is approximately 2 kV. The accuracy of this $\Phi_{||}$ is limited by the finite electron energy resolutions, whose uncertainty is about 0.77 kV if we take the averaged half-width of the used energy channels as errors. Nevertheless, this $\Phi_{||}$ is larger than the electron thermal temperature (Figure 3f). With $e\Phi_{||} \geq kT_{e,||}$, the density of parallel electrons decrease after they enter into the $\Phi_{||}$ region from the right side (Figure 4i), and the electron density at the anti-parallel direction increases from the left to right after the energy gain from $\Phi_{||}$ (Figure 4j).

As $\Phi_{||}$ is the primary factor for electron dynamics in guide-field reconnection, we then derive a functional form of $\Phi_{||}$ here. First, we make two assumptions: (a) $E_{||}$ is almost in the M–N plane (Figure 4l), so $\Phi_{||}$ is scaled as $\Phi_{||} = \int E_{||} dl \sim \langle E_{||} \rangle L_M$, where L_M is the length of the $\Phi_{||}$ region in the M direction, and $\langle E_{||} \rangle$ is the mean value of $E_{||}$ across the current sheet; and (b) the reconnection structure is stable, so that the following geometry relation, written as $\frac{L_N}{L_M} \sim \frac{B_N}{B_e} \sim \frac{RB_L}{B_e}$, is satisfied, where L_N is the length of the $\Phi_{||}$ region in the N direction, and R is the normalized reconnection ratio. Meanwhile, if taking the ratio between $\langle E_{||} \rangle$ and E_R as f , $\langle E_{||} \rangle$ is expressed as $\langle E_{||} \rangle \sim f * E_R \sim f * RV_{A,in} B_L$. Combining the relations above, we have

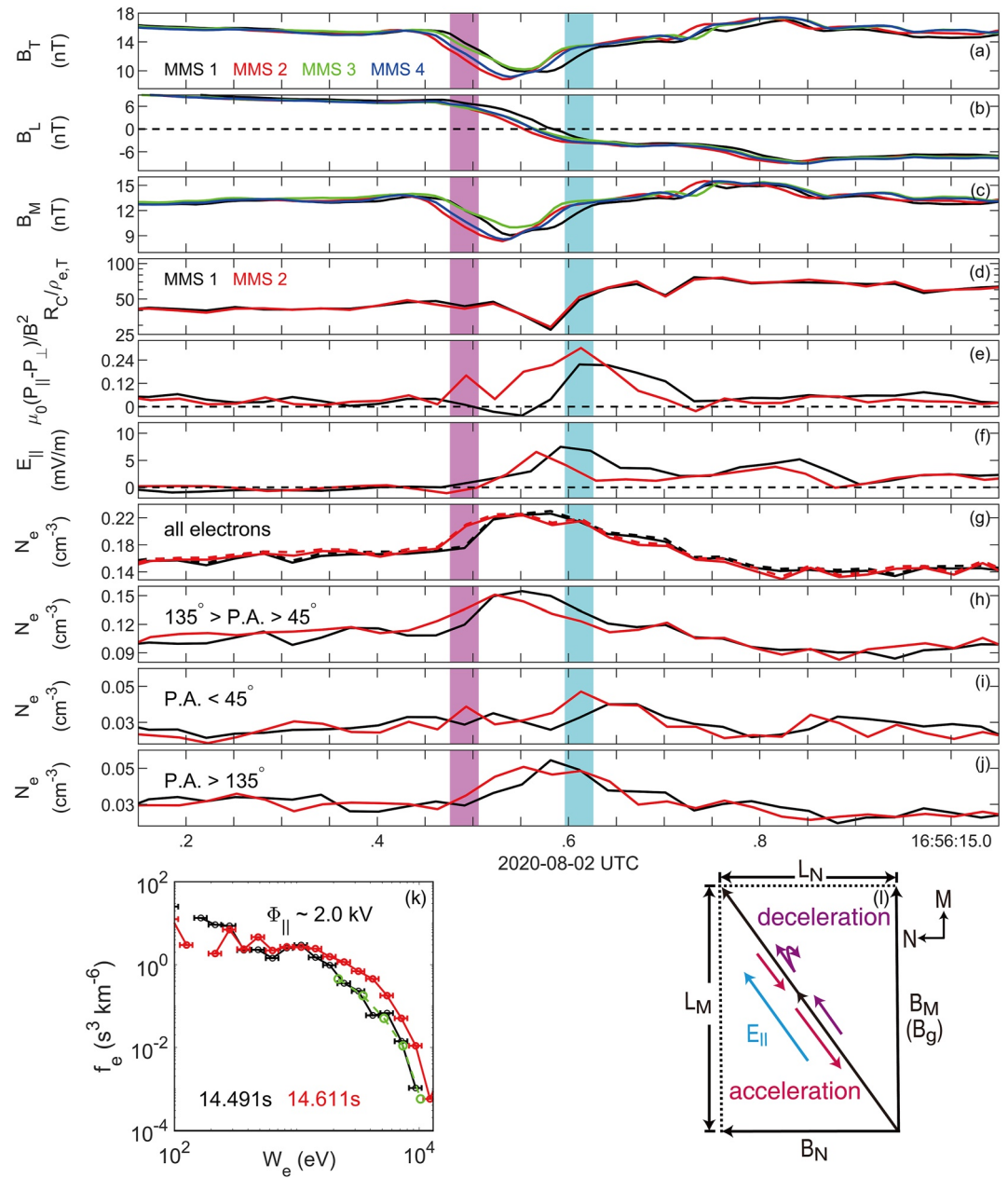


Figure 4. MMS observations of guide-field reconnection. Panels are (a) the total magnetic field (B_T), (b) The magnetic B_L component, (c) The magnetic B_M component, (d) ratio of the magnetic curvature radius and the electron thermal gyro-radius, (e) the electron firehose parameter, (f) the parallel electric field, (g) the total electron density and (h–j) the partial densities at different pitch angles. Colors indicate observations from different MMS spacecraft. (k) MMS 1 observations of the electron phase space density at 180° pitch angle adopted from the magenta and cyan region in the above panels. (l) Schematic of the 2D structure of the observed guide-field reconnection in the M–N plane.

$$\Phi_{\parallel} \sim \langle E_{\parallel} \rangle L_M \sim f * V_{A,in} B_g L_N. \quad (1)$$

This equation indicates that Φ_{\parallel} is related to B_g , but not to the reconnection ratio R . Furthermore, if taking L_N as the width of the electron current layer in reconnection, L_N is 3 ~ 5 times of the electron inertial length (d_e) based on previous studies (W.-Y. Li et al., 2021; Tang et al., 2022), or similarly the electron thermal gyro-radius (ρ_e) in strong guide-field reconnection ($L_N \sim 30$ –70 km). The ratio between the inferred E_{\parallel} and E_R (f) is about 4 ~ 13, consisting with MMS observations.

3. Discussion and Summary

In this study, we have investigated detailed electron dynamics in guide-field reconnection, which is observed at the center of a flux rope in the magnetotail. Due to the presence of a large E_{\parallel} in the vicinity of the reconnection region, electrons are accelerated/decelerated when entering the E_{\parallel} region from different directions. As the related acceleration potential (Φ_{\parallel}) is found to satisfy $e\Phi_{\parallel} \geq kT_{e,\parallel}$, some electrons can significantly reduce their parallel speed to ~ 0 to form more isotropic electron distributions at one side of the electron current sheet, and therefore create a density peak inside the electron current sheet. By deriving a function for Φ_{\parallel} , we infer the magnitude of E_{\parallel} is 4 \sim 13 times of E_R , consistent with MMS observations. As the large E_{\parallel} is only observed in the electron current sheet, the related Φ_{\parallel} is integrated in a limited region accordingly. Thus this Φ_{\parallel} is different with the acceleration potential derived from an analytical model on the electron anisotropy (Egedal et al., 2013; Le et al., 2009), which is present over large spatial scales in reconnection. This potential can effectively accelerate electrons along separatrixes (Norgren et al., 2020) and modify the plasma density structures in guide-field reconnection (Wetherton et al., 2021). The relation between these two parallel potentials should be explored in the future.

Then the question comes to why there is a large E_{\parallel} in guide-field reconnection. In a kinetic simulation of reconnection with a moderate guide-field, a large E_{\parallel} , which is cocurrent with the electron current sheet, is generated to balance the parallel electron pressure gradient of the two electron populations across this current sheet: one is relatively isotropic, and the other is anisotropic (Wetherton et al., 2022). In the moderate guide-field reconnection (the normalized guide field is ~ 0.5), the electron firehose condition is marginally approached, responsible for the unmagnetized isotropic electron population. However, it is not the case for the strong guide-field reconnection here (the normalized guide field is ~ 1.5), as the electron firehose condition is not satisfied (Figure 4e), and electrons are roughly magnetized throughout the current sheet (Figure 4d). But relatively isotropic and anisotropic electron populations at the two sides of the electron current sheet are still observed (Figure 3h), which can lead a large E_{\parallel} in a similar way. We further test this mechanism by checking the relation $E_{\parallel} \sim \frac{\Phi_{\parallel}}{L_M} \sim \frac{\Delta P_{e,\parallel}}{n_e e L_M}$. We find $\frac{\Delta P_{e,\parallel}}{n_e} \sim 0.028$ nPa, and $n_e \sim 0.17$ cm $^{-3}$ is about 1.01 keV, which is comparable with $e\Phi_{\parallel}$ (2.0 ± 0.77 keV). The discrepancy can be attributed to several reasons. First, we assume E_{\parallel} is mostly in the M-N plane to get the checked relation above, but E_{\parallel} is not always in this plane from observations (Wilder et al., 2018). Second, the full pressure tensor effects are not included (Wetherton et al., 2022).

Based on MMS observations, the necessary condition for the generation of relatively isotropic electron distributions at one side of the electron current sheet in strong guide-field reconnection is $e\Phi_{\parallel} \geq kT_{e,\parallel}$. Considering the derived function of Φ_{\parallel} , the thickness of the electron current sheet (L_N is g times of d_e or ρ_e), and the magnitude of the normalized guide field ($B_g/B_L = \alpha$), we have

$$2\sqrt{\frac{m_e}{m_i}} \frac{fg}{\sqrt{1+\alpha^{-2}}} \geq \beta_e, \sqrt{\beta_e}. \quad (2)$$

The choosing of β_e and $\sqrt{\beta_e}$ at the right side of the equation depends on the scaling of L_N . This equation shows that the electron β_e is an important parameter for the generation of relatively isotropic electron distributions in strong guide-field reconnection. In this event, the left side of Equation 2 is estimated from 0.58 to 2.14, and β_e is about 0.71, showing that Equation 2 is well satisfied. We note β_e here is locally adopted at the electron current sheet, which is different from the asymptotic β_e in the inflow region, but it still indicates that only in a proper β_e region, a large parallel electric field can appear. Recently, direct scaled comparisons of guide-field reconnection have been performed between ground experiments and in situ space observations (Fox et al., 2018). Although they have shared many common features, the large parallel electric field generated in the ground experiments is much smaller than that in MMS observations, and Fox et al. (2018) has proposed several possibilities, which includes the plasma beta effect, to explain this discrepancy. Our analysis shows that Equation 2 could be applicable to explain the puzzling issue of the absence of a large parallel electric field in guide-field reconnection in ground experiments (Fox et al., 2018).

Data Availability Statement

MMS data are available at the MMS Science Data Center (<https://lasp.colorado.edu/mms/sdc/public/about/browse-wrapper/>). The MMS data are analyzed using the IRFU-Matlab package (<https://github.com/irfu/irfu-matlab>).

Acknowledgments

We thank Dr. R.-S. Wang for helpful discussions. This work was supported by the National Natural Science Foundation of China (Grants 42188101, 42122032, 41974196, 42274211, 41974170 and 42150105) and the Specialized Research Fund for State Key Laboratories of China. B.-B. T. (2019153) was supported by the Youth Innovation Promotion Association of the Chinese Academy of Sciences.

References

- Burch, J., Torbert, R., Phan, T., Chen, L.-J., Moore, T., Ergun, R., et al. (2016). Electron-scale measurements of magnetic reconnection in space. *Science*, 352(6290), aaf2939. <https://doi.org/10.1126/science.aaf2939>
- Drake, J., Swisdak, M., Cattell, C., Shay, M., Rogers, B., & Zeiler, A. (2003). Formation of electron holes and particle energization during magnetic reconnection. *Science*, 299(5608), 873–877. <https://doi.org/10.1126/science.1080333>
- Eastwood, J., Mistry, R., Phan, T., Schwartz, S., Ergun, R., Drake, J., et al. (2018). Guide field reconnection: Exhaust structure and heating. *Geophysical Research Letters*, 45(10), 4569–4577. <https://doi.org/10.1029/2018gl077670>
- Eastwood, J., Shay, M., Phan, T., & Øieroset, M. (2010). Asymmetry of the ion diffusion region hall electric and magnetic fields during guide field reconnection: Observations and comparison with simulations. *Physical Review Letters*, 104(20), 205001. <https://doi.org/10.1103/physrevlett.104.205001>
- Egedal, J., Le, A., & Daughton, W. (2013). A review of pressure anisotropy caused by electron trapping in collisionless plasma, and its implications for magnetic reconnection. *Physics of Plasmas*, 20(6), 061201. <https://doi.org/10.1063/1.4811092>
- Ergun, R., Tucker, S., Westfall, J., Goodrich, K., Malaspina, D., Summers, D., et al. (2016). The axial double probe and fields signal processing for the MMS mission. *Space Science Reviews*, 199(1–4), 167–188. <https://doi.org/10.1007/s11214-014-0115-x>
- Fox, W., Wilder, F. D., Eriksson, S., Jara-Almonte, J., Pucci, F., Yoo, J., et al. (2018). Energy conversion by parallel electric fields during guide field reconnection in scaled laboratory and space experiments. *Geophysical Research Letters*, 45(23), 12–677. <https://doi.org/10.1029/2018gl079883>
- Genestreti, K., Burch, J., Cassak, P., Torbert, R., Ergun, R., Varsani, A., et al. (2017). The effect of a guide field on local energy conversion during asymmetric magnetic reconnection: Mms observations. *Journal of Geophysical Research: Space Physics*, 122(11), 11–342. <https://doi.org/10.1002/2017ja024247>
- Goldman, M., Lapenta, G., Newman, D., Markidis, S., & Che, H. (2011). Jet deflection by very weak guide fields during magnetic reconnection. *Physical Review Letters*, 107(13), 135001. <https://doi.org/10.1103/physrevlett.107.135001>
- Kacem, I., Jacquety, C., Génot, V., Lavraud, B., Vernisse, Y., Marchaudon, A., et al. (2018). Magnetic reconnection at a thin current sheet separating two interlaced flux tubes at the Earth's magnetopause. *Journal of Geophysical Research: Space Physics*, 123(3), 1779–1793. <https://doi.org/10.1002/2017ja024537>
- Khotyaintsev, Y. V., Graham, D., Steinvaal, K., Alm, L., Vaivads, A., Johlander, A., et al. (2020). Electron heating by Debye-scale turbulence in guide-field reconnection. *Physical Review Letters*, 124(4), 045101. <https://doi.org/10.1103/physrevlett.124.045101>
- Le, A., Egedal, J., Daughton, W., Fox, W., & Katz, N. (2009). Equations of state for collisionless guide-field reconnection. *Physical Review Letters*, 102(8), 085001. <https://doi.org/10.1103/physrevlett.102.085001>
- Le, A., Egedal, J., Ohia, O., Daughton, W., Karimabadi, H., & Lukin, V. (2013). Regimes of the electron diffusion region in magnetic reconnection. *Physical Review Letters*, 110(13), 135004. <https://doi.org/10.1103/physrevlett.110.135004>
- Li, W.-Y., Khotyaintsev, Y. V., Tang, B.-B., Graham, D., Norgren, C., Vaivads, A., et al. (2021). Upper-hybrid waves driven by meandering electrons around magnetic reconnection x line. *Geophysical Research Letters*, 48(16), e2021GL093164. <https://doi.org/10.1029/2021gl093164>
- Li, X., Wang, R., & Lu, Q. (2022). Division of magnetic flux rope via magnetic reconnection observed in the magnetotail. *Geophysical Research Letters*, e2022GL101084. <https://doi.org/10.1029/2022GL101084>
- Lindqvist, P.-A., Olsson, G., Torbert, R., King, B., Granoff, M., Rau, D., et al. (2016). The spin-plane double probe electric field instrument for MMS. *Space Science Reviews*, 199(1–4), 137–165. <https://doi.org/10.1007/s11214-014-0116-9>
- Norgren, C., Hesse, M., Graham, D. B., Khotyaintsev, Y. V., Tenfjord, P., Vaivads, A., et al. (2020). Electron acceleration and thermalization at magnetotail separatrices. *Journal of Geophysical Research: Space Physics*, 125(4), e2019JA027440. <https://doi.org/10.1029/2019ja027440>
- Øieroset, M., Phan, T., Drake, J., Eastwood, J., Fuselier, S., Strangeway, R., et al. (2019). Reconnection with magnetic flux pileup at the interface of converging jets at the magnetopause. *Geophysical Research Letters*, 46(4), 1937–1946. <https://doi.org/10.1029/2018gl080994>
- Øieroset, M., Phan, T., Haggerty, C., Shay, M. A., Eastwood, J. P., Gershman, D. J., et al. (2016). Mms observations of large guide field symmetric reconnection between colliding reconnection jets at the center of a magnetic flux rope at the magnetopause. *Geophysical Research Letters*, 43(11), 5536–5544. <https://doi.org/10.1002/2016gl069166>
- Phan, T., Paschmann, G., Gosling, J., Øieroset, M., Fujimoto, M., Drake, J., & Angelopoulos, V. (2013). The dependence of magnetic reconnection on plasma β and magnetic shear: Evidence from magnetopause observations. *Geophysical Research Letters*, 40(1), 11–16. <https://doi.org/10.1029/2012gl054528>
- Pollock, C., Moore, T., Jacques, A., Burch, J., Gliese, U., Saito, Y., et al. (2016). Fast plasma investigation for magnetospheric multiscale. *Space Science Reviews*, 199(1–4), 331–406. <https://doi.org/10.1007/s11214-016-0245-4>
- Russell, C., Anderson, B., Baumjohann, W., Bromund, K., Dearborn, D., Fischer, D., et al. (2016). The magnetospheric multiscale magnetometers. *Space Science Reviews*, 199(1–4), 189–256. <https://doi.org/10.1007/s11214-014-0057-3>
- Sonnerup, B. U., Hasegawa, H., Teh, W.-L., & Hau, L.-N. (2006). Grad-shafranov reconstruction: An overview. *Journal of Geophysical Research*, 111(A9), A09204. <https://doi.org/10.1029/2006ja011717>
- Swisdak, M., Drake, J., Shay, M., & McIlhargey, J. (2005). Transition from antiparallel to component magnetic reconnection. *Journal of Geophysical Research*, 110(A5), A05210. <https://doi.org/10.1029/2004ja010748>
- Swisdak, M., Rogers, B., Drake, J., & Shay, M. (2003). Diamagnetic suppression of component magnetic reconnection at the magnetopause. *Journal of Geophysical Research*, 108(A5), 1218. <https://doi.org/10.1029/2002ja009726>
- Tang, B.-B., Li, W., Khotyaintsev, Y. V., Graham, D. B., Gao, C., Chen, Z., et al. (2022). Fine structures of the electron current sheet in magnetotail guide-field reconnection. *Geophysical Research Letters*, 49(9), e2021GL097573. <https://doi.org/10.1029/2021gl097573>
- Tang, B.-B., Li, W., Le, A., Graham, D., Wu, Y., Wang, C., et al. (2020). Electron mixing and isotropization in the exhaust of asymmetric magnetic reconnection with a guide field. *Geophysical Research Letters*, 47(14), e2020GL087159. <https://doi.org/10.1029/2020gl087159>
- Wang, S., Wang, R., Lu, Q., Russell, C., Ergun, R., & Wang, S. (2021). Large-scale parallel electric field co-located in an extended electron diffusion region during the magnetosheath magnetic reconnection. *Geophysical Research Letters*, 48(23), e2021GL094879. <https://doi.org/10.1029/2021gl094879>
- Wetherton, B. A., Egedal, J., Le, A., & Daughton, W. (2021). Anisotropic electron fluid closure validated by in situ spacecraft observations in the far exhaust of guide-field reconnection. *Journal of Geophysical Research: Space Physics*, 126(1), e2020JA028604. <https://doi.org/10.1029/2020ja028604>
- Wetherton, B. A., Egedal, J., Le, A., & Daughton, W. (2022). Generation of a strong parallel electric field and embedded electron jet in the exhaust of moderate guide field reconnection. *Geophysical Research Letters*, 49(14), e2022GL098907. <https://doi.org/10.1029/2022gl098907>

- Wilder, F., Ergun, R., Burch, J., Ahmadi, N., Eriksson, S., Phan, T., et al. (2018). The role of the parallel electric field in electron-scale dissipation at reconnecting currents in the magnetosheath. *Journal of Geophysical Research: Space Physics*, 123(8), 6533–6547. <https://doi.org/10.1029/2018ja025529>
- Wilder, F., Ergun, R., Eriksson, S., Phan, T., Burch, J., Ahmadi, N., et al. (2017). Multipoint measurements of the electron jet of symmetric magnetic reconnection with a moderate guide field. *Physical Review Letters*, 118(26), 265101. <https://doi.org/10.1103/physrevlett.118.265101>
- Zhang, Y., Liu, Z., Shen, C., Fazakerley, A., Dunlop, M., Réme, H., et al. (2007). The magnetic structure of an earthward-moving flux rope observed by cluster in the near-tail. *Annales Geophysicae*, 25(7), 1471–1476. <https://doi.org/10.5194/angeo-25-1471-2007>